MBTT Inversion with a Poor Initial Velocity Background: Optimization Strategies? Density of Shots?

François Clément

INRIA

INSTITUT NATIONAL DE RECHERCHE EN INFORMATIQUE ET EN AUTOMATIQUE

MBTT Inversion with a Poor Initial Velocity Background: Optimization Strategies? Density of Shots?

François Clément

N ° 3657

Avril 1999

THÈME 4

ISSN 0249-6399

INRIA
ROCQUENCOURT

MBTT Inversion with a Poor Initial Velocity Background: Optimization Strategies? Density of Shots?

François Clément*

Thème 4 — Simulation et optimisation
de systèmes complexes
Projet Estime

Rapport de recherche n ° 3657 — Avril 1999 — 17 pages

Abstract: The Migration-Based TravelTime (MBTT) reformulation of the classical least-squares waveform inversion problem enlarges the attraction domain for the global minimum of the data misfit function, but does not make it convex. Systematic experimentation on the possible strategies to perform the minimization of the criterion with respect to the new MBTT unknowns (the propagator and the time reflectivity) is presented on a non-layered synthetic example with a finite-difference acoustic simulator. The influence of the amount of available data on the enlargement of the attraction domain is also investigated.

Key-words: inverse problem, time formulation, acoustic waves, finite difference, optimization, background velocity inversion, reflectivity inversion

(Résumé : tsvp)

This research was carried out as part of the Seismic Inversion, Geophysical Modeling and Applications Consortium. The authors hereby acknowledge the support provided by the sponsors of the SIGMA Consortium.

* Projet Estime

Inversion en temps de parcours par migration avec un mauvais modèle de vitesse initial : stratégie d'optimisation ? densité de tir ?

Résumé : L'inversion par forme d'onde étant formulée comme un problème aux moindres carrés classique, la reformulation en temps de parcours par migration élargit le domaine d'attraction du minimum global de la fonction d'écart aux données, mais sans la rendre convexe. Une expérimentation systématique des stratégies d'optimisation possibles pour la minimisation du critère par rapport aux nouvelles inconnues (propagateur et réflectivité en temps) est présentée sur un exemple synthétique non stratifié avec un simulateur acoustique par différences finies. L'influence de la masse de données disponibles sur l'élargissement du domaine d'attraction est également étudiée.

Mots-clé : problème inverse, formulation en temps, ondes acoustiques, différences finies, optimisation, inversion du modèle de vitesse, inversion de la réflectivité

1 Introduction

Waveform inversion of reflection seismic data has been hindered by the extremely poor behavior of the Classical Least-Squares (CLS) data misfit with respect to the low-frequency components of the slowness model: saturation effects and local minima have prevented local optimization algorithms to get close to the global minimum.

Differential Semblance, see [6], consists in using another criterion to be minimized: the semblance of the migrated images which is measured in the time domain after a forward modeling step. This approach has the advantage of having well-defined and smooth high-frequency asymptotics. Migration-Based TravelTime (MBTT) approach, see [2], consists in a change of unknowns for the CLS data misfit. Numerical results show that the MBTT change of unknowns enlarges the attraction domain for the global minimum of the least-squares criterion, without making it convex, but this is enough to allow the minimization of the misfit by a local technique, see [1, 4].

In this work, I try to give clues about the question: how far can the initial guess be? The idea is to consider an initial guess which gives acceptable inversion results with the MBTT formulation (here a constant gradient to retrieve a model with lateral variations), and then to investigate on a wide variety of possible ways to minimize the misfit in order to try to define an "optimal minimization strategy". Then, the initial guess is degraded (here from a constant gradient to a constant function) and the influence of the density of shots on the inversion results is studied for the previous optimal strategy.

All these numerical experiments are made with a 2D finite-difference acoustic forward modeling on synthetic data computed from a non-layered model. All the numerical results showed in this paper have taken about 4 months of computation on DEC Alpha workstations, this represent some $1.5\,10^{15}$ floating point operations at the average speed of 150 Mflops.

2 Migration-Based TravelTime formulation

In this work, I consider forward modeling by a 2D finite-difference acoustic simulator in media with known smooth density. I only recall here the principle of the Migration-Based TravelTime (MBTT) formulation of waveform inversion. More details can be found in [3].

Let d a collection of shot gathers to be inverted, ν the current slowness and c the corresponding collection of synthetic shot gathers. The least-squares waveform data misfit J associated with ν is

$$J = \frac{1}{2}\|d - c\|^2, \tag{1}$$

where $\|.\|$ is the Euclidean norm for the collection of shot gathers. The Classical Least-Squares (CLS) formulation of waveform inversion is to find $\hat{\nu}$ which minimizes J given by (1) where c is computed from the slowness ν. This formulation suffers from a major flaw: the misfit J has numerous local minima with respect to the low-frequency components of the slowness ν.

The MBTT reformulation consists then in two steps. First, the slowness ν is decomposed into the sum of a smooth part ν_s and a rough part ν_r, respectively parameterized by the propagator p and the depth reflectivity r,

$$\nu = \nu_s(p) + \nu_r(r). \tag{2}$$

Second, for each propagator p, the depth reflectivity r is parameterized by the quantitative migration with smooth background $\nu_s(p)$ of the time reflectivity s,

$$r = \boldsymbol{\mathcal{M}}(p)s. \tag{3}$$

Notice that the time reflectivity s has the same structure as the data d. Finally, the MBTT reformulation of the least-squares waveform inversion is to find $\hat{p}$ and $\hat{s}$ which minimizes J given by (1) where c is computed from the slowness ν obtained from the propagator p and the time

reflectivity s by (2) and (3). This reformulation has the benefit effect of enlarging the domain of attraction for the global minimum of J, and hence allows the use of a local optimization method to minimize the least-squares criterion.

3 Multiscale representation of the propagator

I recall here briefly the construction of the multiscale representation in the space of slownesses. More details can also be found in [3].

Let V be the space of slownesses. It is made of functions bilinearly interpolated on the finite-difference grid Ω_h of the acoustic simulator, *i.e.*, using a tensor product of linear interpolation in both space directions. By dichotomy on the mesh size, I build an embedded sequence of grids

$$\Omega_0 \subset \ldots \subset \Omega_K = \Omega_h. \tag{4}$$

At each scale $k = 0, \ldots, K$, I consider the space V_k of functions bilinearly interpolated on the grid Ω_k. Each space is provided with its canonical local basis of "hat" functions, *i.e.*, which take the value 1 at a given node and zero at all other nodes. This defines an embedded sequence of spaces

$$V_0 \subset \ldots \subset V_K = V. \tag{5}$$

At each scale $k = 1, \ldots, K$, I denote by W_k the canonical supplementary to V_{k-1} in V_k. This defines the following multiscale representation

$$V_k = V_0 \oplus W_1 \oplus \ldots \oplus W_k. \tag{6}$$

Notice that this multiscale representation is not orthonormal: two canonical basis functions are orthogonal one to the other if and only if they have disjoint support; furthermore, the L^2-norm of the basis functions decreases with the scale.

The space V_s for smooth slownesses is chosen as the space of highest scale K_s such that the shot gathers associated with any slowness contain no sizeable reflections. This corresponds to scale 2 for the Synclay model. The propagator p is then the components of the current smooth slowness on the canonical multiscale basis of $V_2 = V_0 \oplus W_1 \oplus W_2$. For the Synclay model, the dimension of the spaces V_0, V_1 and V_2 is respectively 16, 49 and 169, to be compared to the dimension 40401 for the full space V.

4 Influence of the optimization strategy

With the MBTT approach, inversion consists in minimizing the least-squares data misfit J defined by (1) with respect to the unknowns p (propagator) and s (time reflectivity), see section 2. The propagator p is itself decomposed on a multiscale basis, see section 3. Thus, there are many possible ways to intertwine the optimizations with respect to p at various scales and with respect to s.

I have fixed the optimization effort to 60 iterations with respect to p and 30 iterations with respect to s. In all cases, I have tested if these 90 MBTT iterations allowed to get close enough to the global minimum by performing 40 additional iterations with respect to ν. In order to allow a comparison, I have also considered 600 CLS iterations with respect to ν, which represents roughly the same computational cost.

All minimizations have been performed using the `m1qn3` routine developed at INRIA which solves unconstrained minimization problems by a variable-storage quasi-Newton method, see [5]. All experiments have been performed on the 5-shot Synclay data set, see Figure 10, and because of the use of a quantitative migration operator in the MBTT change of unknowns, the time reflectivity is always initialized to the data.

The optimization results are summarized in tables: the decrease of the criterion (normalized by the value $\frac{1}{2}\|d\|^2$), the number of iterations, and the number of function and gradient evaluations. I have always split the part due to the MBTT iterations from the part due to CLS iterations. An effective number of iterations lower than the expected one shows that the optimizer have been unable to do more for that run. A number of evaluations of the function and the gradient higher than the effective number of iterations shows that the optimizer have encountered difficulties during the line search along the descent direction. Qualitative results are obtained from the value of the misfit at the optimum and qualitative results are obtained, by the eye, from a comparison of the slowness at the optimum. For the latter, the criteria are the correctness of the location of the reflectors and the average value of the slowness in the layers in between.

4.1 The optimization strategies

For the MBTT formulation, I have considered four types of strategies: direct (D), multiscale (M), alternate multiscale (MA), and progressive alternate multiscale (MAP), with equal, increasing or decreasing number of iterations at each scale.

The direct strategy corresponds to minimize with respect to the propagator at the highest scale, then with respect to the time reflectivity,

D-MBTT+CLS $60/p_2$, $30/s$, $40/\nu$,

i.e., 60 iterations with respect to p at scale 2, followed by 30 iterations with respect to s, followed by 40 iterations with respect to ν.

The multiscale strategies correspond to minimize with respect to the propagator at the first scales, then at the second scale, and so on ... , then with respect to the time reflectivity,

M_0-MBTT+CLS $20/p_0$, $20/p_1$, $20/p_2$, $30/s$, $40/\nu$,

M_1-MBTT+CLS $10/p_0$, $20/p_1$, $30/p_2$, $30/s$, $40/\nu$,

M_2-MBTT+CLS $30/p_0$, $20/p_1$, $10/p_2$, $30/s$, $40/\nu$.

The alternate multiscale strategies correspond to minimize with respect to the time reflectivity after each minimization with respect to the propagator, and the progressive alternate multiscale strategies correspond to perform several alternate runs at each scale,

MA_0-MBTT+CLS $20/p_0$, $10/s$, $20/p_1$, $10/s$, $20/p_2$, $10/s$, $40/\nu$,

MAP_1-MBTT+CLS $10/p_0$, $5/s$, $10/p_0$, $5/s$, $10/p_1$, $5/s$, $10/p_1$, $5/s$, $10/p_2$, $5/s$, $10/p_2$, $5/s$, $40/\nu$,

MAP_2-MBTT+CLS $5/p_0$, $2/s$, $5/p_0$, $3/s$, $5/p_0$, $2/s$, $5/p_0$, $3/s$, $5/p_1$, $2/s$, $5/p_1$, $3/s$, $5/p_1$, $2/s$, $5/p_1$, $3/s$, $5/p_2$, $2/s$, $5/p_2$, $3/s$, $5/p_2$, $2/s$, $5/p_2$, $3/s$, $40/\nu$,

MA_1-MBTT+CLS $10/p_0$, $5/s$, $20/p_1$, $10/s$, $30/p_2$, $15/s$, $40/\nu$,

MA_2-MBTT+CLS $10/p_0$, $15/s$, $20/p_1$, $10/s$, $30/p_2$, $5/s$, $40/\nu$,

MA_3-MBTT+CLS $30/p_0$, $5/s$, $20/p_1$, $10/s$, $10/p_2$, $15/s$, $40/\nu$,

MA_4-MBTT+CLS $30/p_0$, $15/s$, $20/p_1$, $10/s$, $10/p_2$, $5/s$, $40/\nu$.

For the CLS formulation, I have only considered the simple strategy,

S-CLS $100/\nu$, $100/\nu$, $100/\nu$, $100/\nu$, $100/\nu$, $100/\nu$.

strategy	normalized criterion	iterations	evaluations
D-MBTT+CLS	0.538↘0.0698↘0.00808	90+40	95+42
M_0-MBTT+CLS	0.538↘0.0705↘0.00679	90+40	98+43
M_1-MBTT+CLS	0.538↘0.0724↘0.0104	90+40	100+42
M_2-MBTT+CLS	0.538↘0.077 ↘0.00601	85+40	98+43
MA_0-MBTT+CLS	0.538↘0.0578↘0.00271	81+40	104+43
MAP_1-MBTT+CLS	0.538↘0.073 ↘0.00373	87+40	110+41
MAP_2-MBTT+CLS	0.538↘0.0697↘0.00314	90+40	134+41
MA_1-MBTT+CLS	0.538↘0.0704↘0.0109	83+40	99+43
MA_2-MBTT+CLS	0.538↘0.0617↘0.00348	90+40	102+42
MA_3-MBTT+CLS	0.538↘0.0698↘0.00725	85+40	105+42
MA_4-MBTT+CLS	0.538↘0.0658↘0.00273	81+40	101+43
S-CLS	1 ↘0.003	0+600	0+646

Table 1: Optimization reports for the inversion of the 5-shot Synclay data starting from the ramp slowness.

4.2 Results obtained from a ramp

First, I consider the initial propagator (or slowness) to be the linear ramp which takes the correct top and bottom values, *i.e.*, 0.67 s/km and 0.25 s/km. This ramp does not present the lateral variations of the Synclay model, and hence it is kinematically quite far from the Synclay slowness, see figure 1 (top left and top right).

From Table 1 and Figure 1, one sees that the D and M_x strategies are ranking as follows:

quantitatively, $M_2 > M_0 > D \gg M_1$,
qualitatively, $M_2 > M_0 \gg M_1 \gg D$,

where an $=$ sign denotes comparable performances and the number of $>$ signs denotes the importance of the gap between the two strategies. This shows the interest of the multiscale representation of the propagator for minimization, and furthermore, that it is very important to decrease the number of iterations with respect to p as the scale increases, *i.e.*, to make the strongest effort on the propagator at the lowest scale.

From Table 1 and Figures 2 and 3, one sees that the M_2, MA_x and MAP_x strategies are ranking as follows:

quantitatively, $MA_0 = MA_4 = MAP_2 = MA_2 > MAP_1 \gg M_2 > MA_3 \gg MA_1$,
qualitatively, $MA_3 > MA_0 = MA_4 > M_2 \gg MAP_1 > MAP_2 = MA_1 = MA_2$.

Apparently, quantitative and qualitative results can disagree. Of course, with this synthetic example which has a poor reflectivity content and in the case of 5 shots only, the qualitative results are more significant. This shows that it is also important to alternate minimizations with respect to the propagator and with respect to the time reflectivity at each scale; but, certainly because the optimizer needs a minimum number of iterations to build a correct approximation to the Hessian of the misfit, a too small number of iterations at each run degrades the performances. Furthermore, it seems important to increase the number of iterations with respect to s as the scale increases, *i.e.*, to increase the effort on the time reflectivity as the kinematics is recovered.

In Figure 4, one sees that the S-CLS strategy cannot make the optimizer significantly change the kinematics of the initial ramp, hence the deep reflectors are misplaced. The fact that layers are still visible, and that the criterion is very low at the optimum, *i.e.*, that the data are explained, is due to the conjunction of the use of a small number of shots and of an initial guess which is close enough to the solution. This shows that the MBTT change of unknowns enlarges the domain of attraction for the global minimum of the least-squares data misfit, even for the inversion of only 5 shots when starting from a ramp.

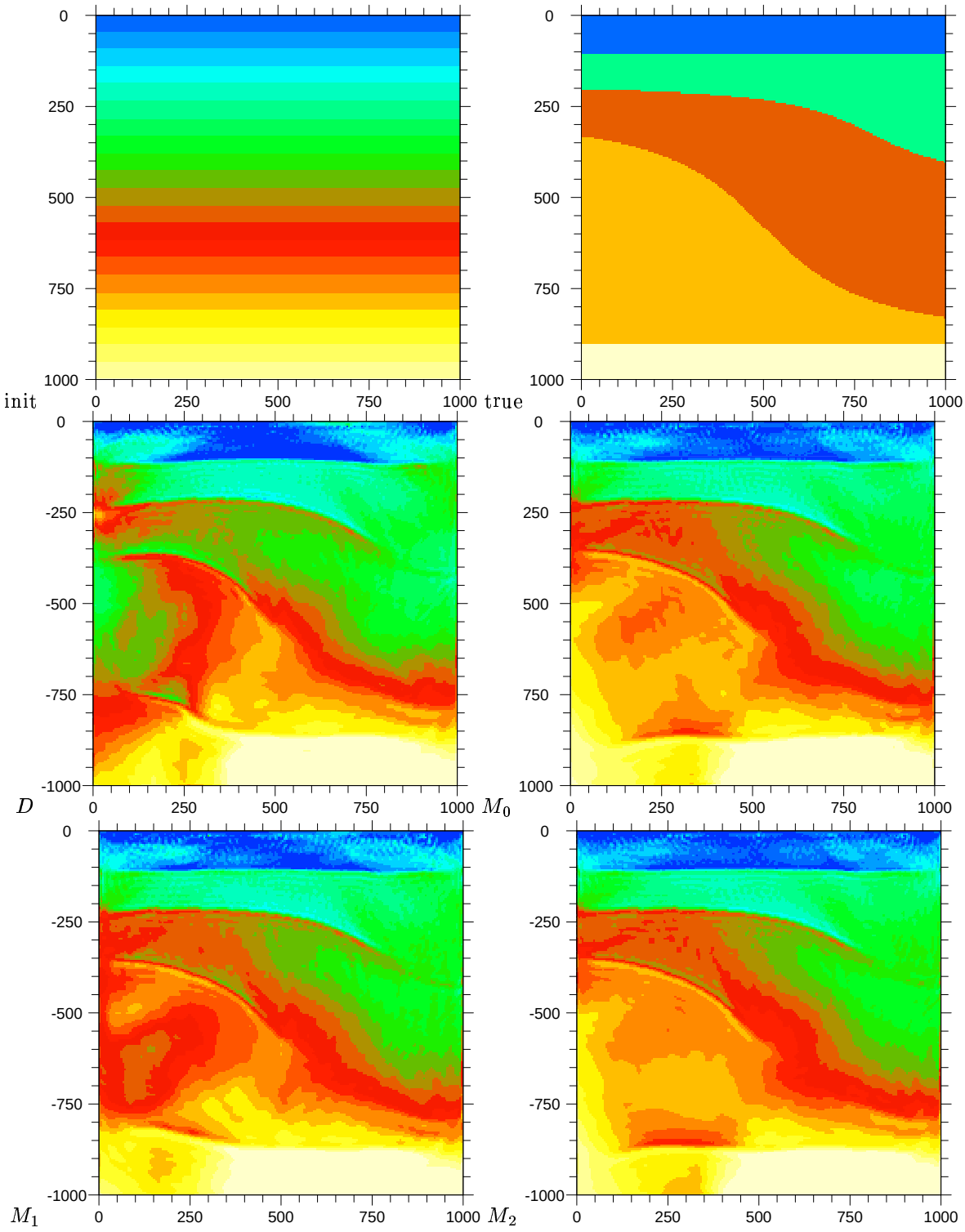

Figure 1: Full slowness after minimization from the ramp for the strategies D-MBTT+CLS, M_0-MBTT+CLS, M_1-MBTT+CLS and M_2-MBTT+CLS.

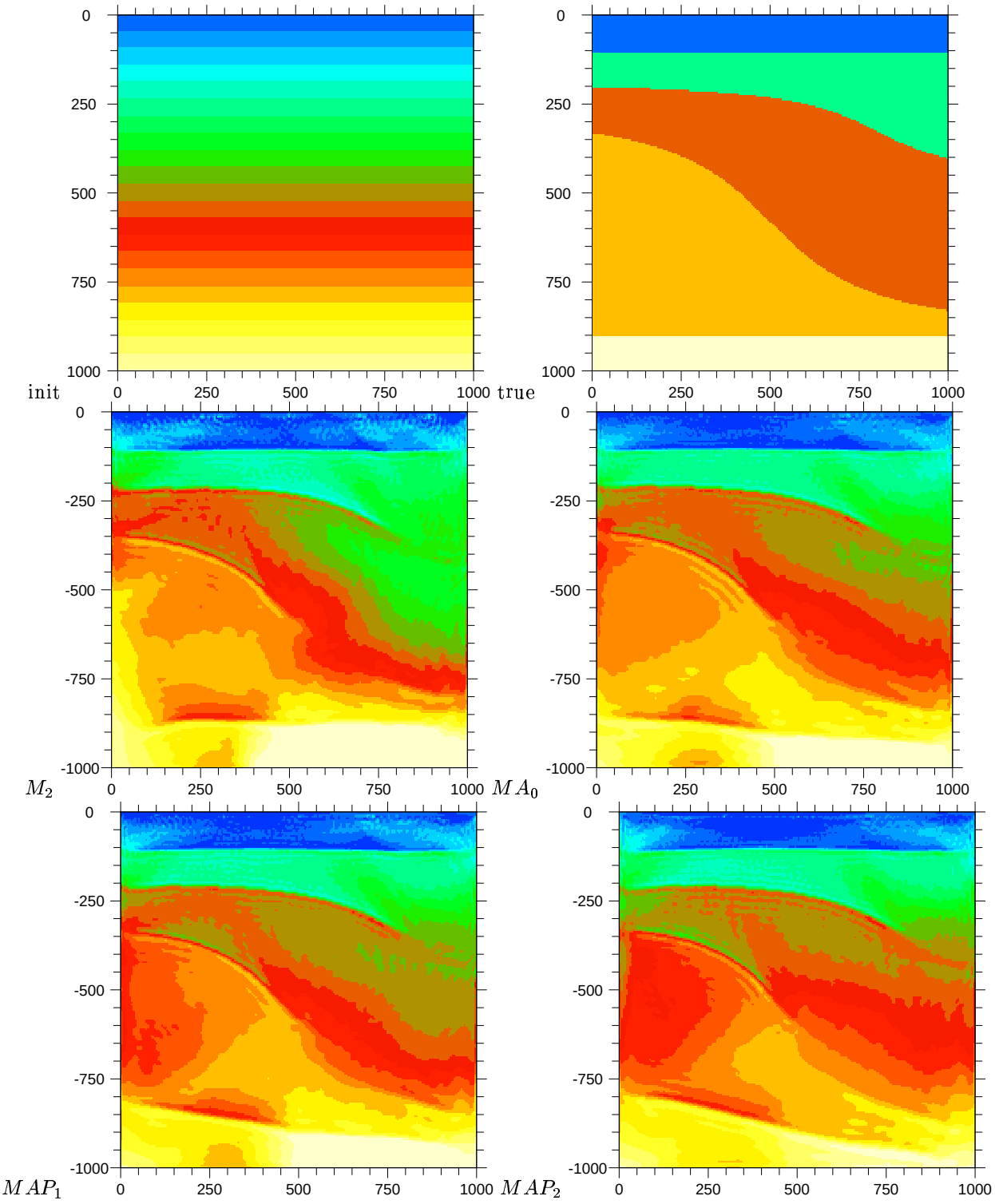

Figure 2: Full slowness after minimization from the ramp for the strategies M_2-MBTT+CLS, MA_0-MBTT+CLS, MAP_1-MBTT+CLS and MAP_2-MBTT+CLS.

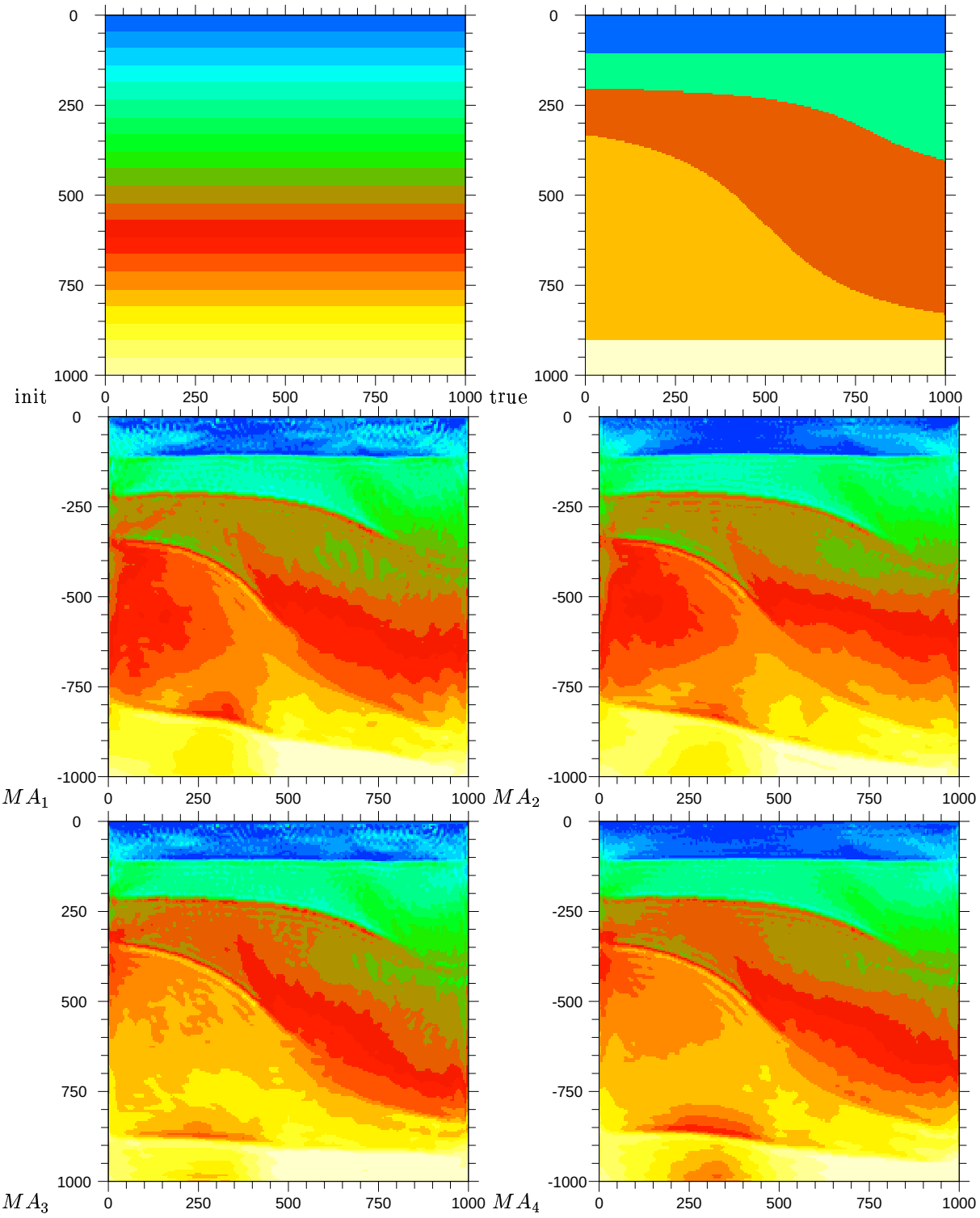

Figure 3: Full slowness after minimization from the ramp for the strategies MA_1-MBTT+CLS, MA_2-MBTT+CLS, MA_3-MBTT+CLS and MA_4-MBTT+CLS.

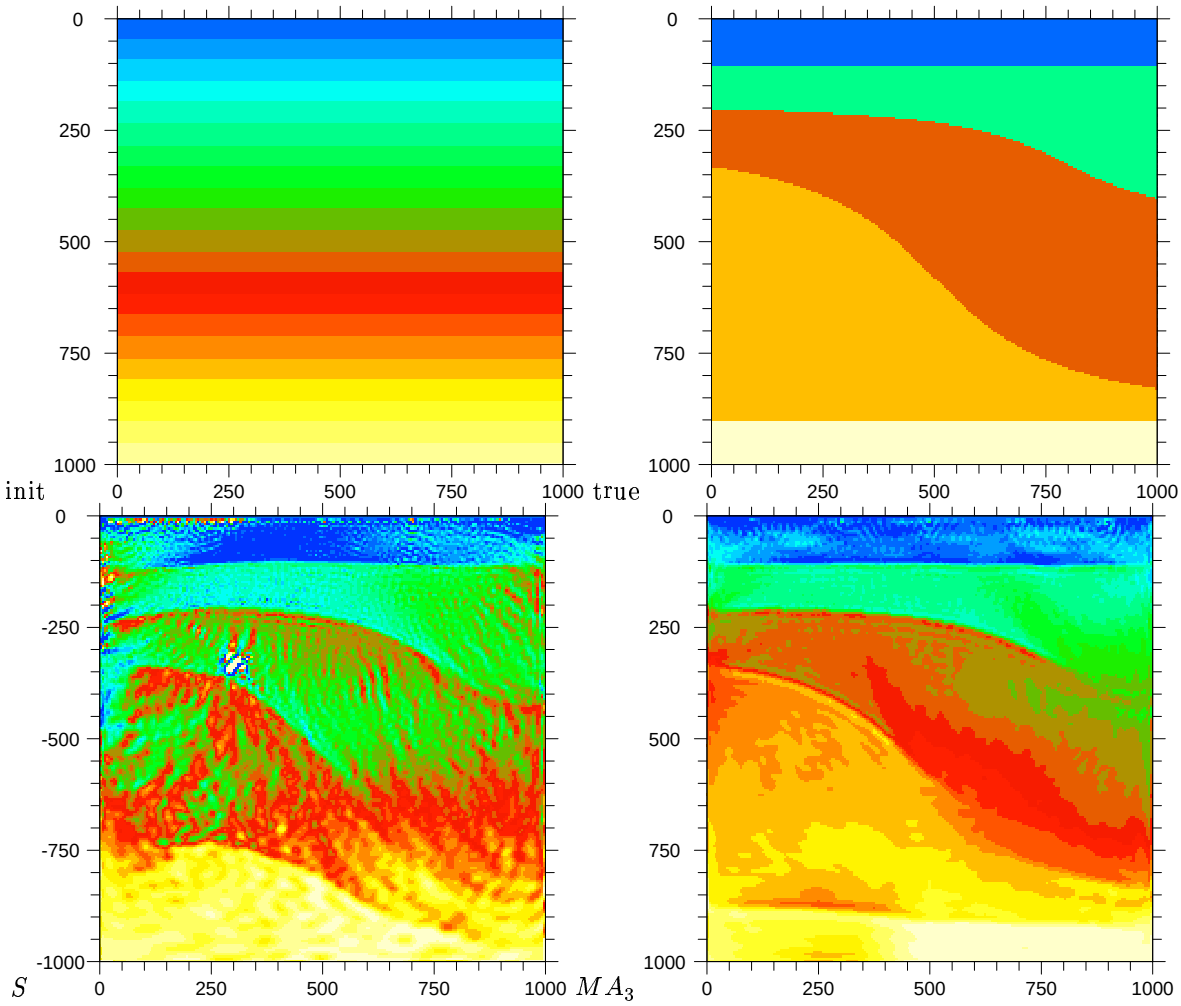

Figure 4: Full slowness after minimization from the ramp for the strategies S-CLS and MA_3-MBTT+CLS.

4.3 Results obtained from a constant

I consider now the initial propagator (or slowness) to be the constant which takes the correct mean value, *i.e.*, 0.4 s/km. This constant does not present any of the variations of the Synclay model, and hence it is kinematically very far from the Synclay slowness, see Figure 5 (top left and top right).

Table 2 shows that, for all MBTT strategies, quantitative results are not significantly different from those obtained from the ramp, but the S-CLS strategy is now unable to explain the data. Figure 5 shows that qualitative results are significantly worse than those obtained from the ramp (deep reflector are misplaced), but also that the MBTT formulation is still able to build a reasonable estimation of the slowness when inverting only 5 shots starting from the very poor constant slowness, which is still better than the estimation obtained by the S-CLS strategy from the ramp.

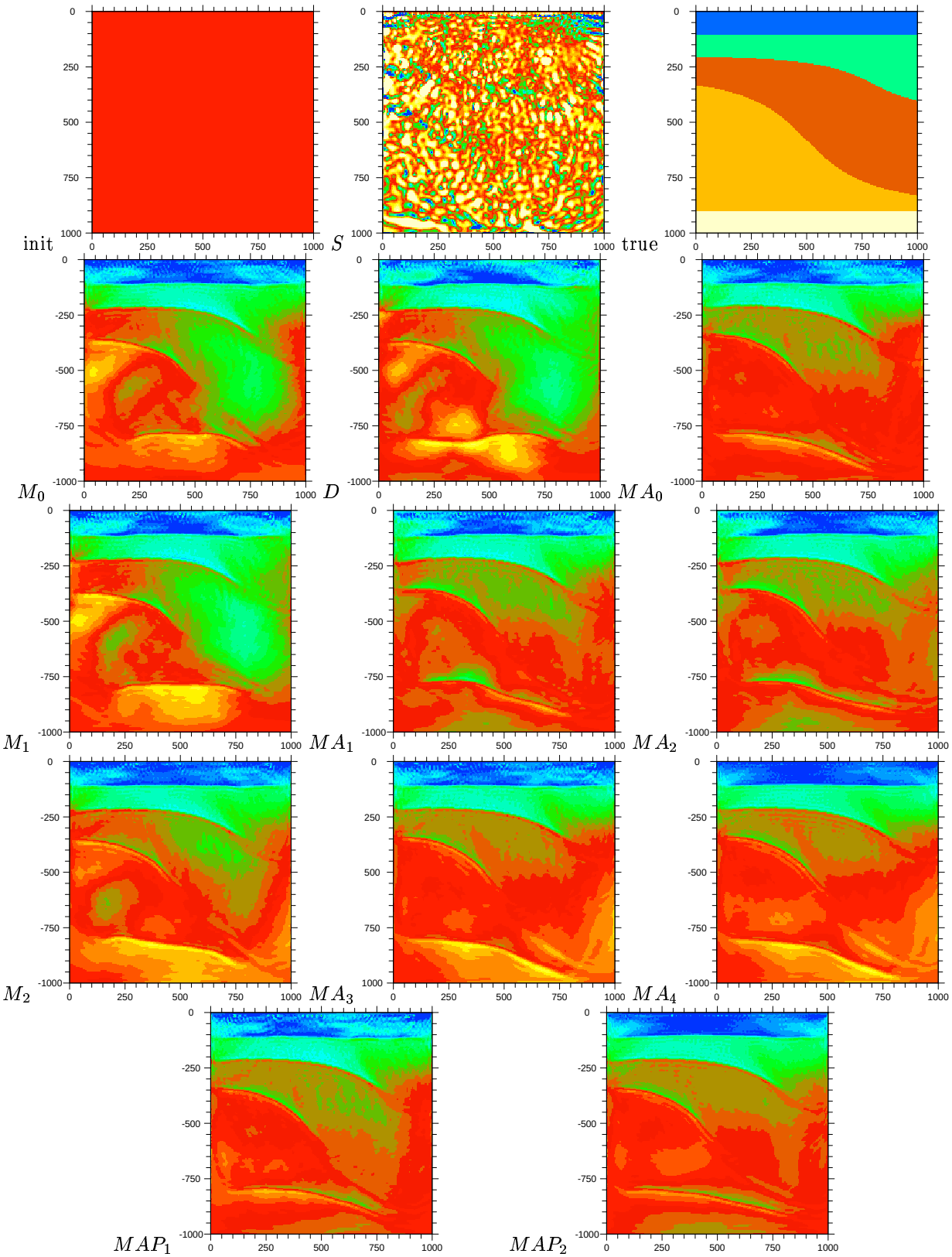

Figure 5: Full slowness after minimization from the constant for all strategies.

strategy	normalized criterion	iterations	evaluations
D-MBTT+CLS	0.786$\searrow$0.0777$\searrow$0.0172	90+40	97+42
M_0-MBTT+CLS	0.786$\searrow$0.0751$\searrow$0.0097	90+40	103+43
M_1-MBTT+CLS	0.786$\searrow$0.0761$\searrow$0.0123	90+40	102+41
M_2-MBTT+CLS	0.786$\searrow$0.0811$\searrow$0.00816	90+40	104+42
MA_0-MBTT+CLS	0.786$\searrow$0.0758$\searrow$0.0115	90+40	106+42
MAP_1-MBTT+CLS	0.786$\searrow$0.085 $\searrow$0.0156	90+40	116+43
MAP_2-MBTT+CLS	0.786$\searrow$0.0764$\searrow$0.00436	89+40	150+43
MA_1-MBTT+CLS	0.786$\searrow$0.0738$\searrow$0.0143	90+40	106+42
MA_2-MBTT+CLS	0.786$\searrow$0.0816$\searrow$0.0104	90+40	106+43
MA_3-MBTT+CLS	0.786$\searrow$0.0738$\searrow$0.0115	90+40	108+42
MA_4-MBTT+CLS	0.786$\searrow$0.0685$\searrow$0.00369	90+40	108+41
S-CLS	1 $\searrow$0.152	0+501	0+549

Table 2: Optimization reports for the inversion of the 5-shot Synclay data starting from the constant slowness.

5 Influence of the density of shots

In the last section, I have shown that the MBTT formulation was significantly enlarging the domain of attraction for the global minimum of the least-squares data misfit, and that, among the wide variety of possible optimization strategies, it was important to perform an alternate multiscale minimization which progressively transfers the effort from the propagator unknown to the time reflectivity unknown as the representation of the propagator is refined. But, when starting from a very poor initial propagator guess, MBTT inversion was only able to recover the upper fourth of the Synclay model. The next step is to test if an increase in the amount of available data can improve the inversion results. The influence of the farest available offset is let to further research, and I test in this section if an increase in the density of shots is able to improve the inversion results obtained from the same constant of value 0.4 s/km with the MA_3-MBTT+CLS strategy.

Figure 6 shows scans of the least-squares criterion, for both CLS and MBTT formulations, on the triangle in the space V_s of smooth background slownesses which vertices are the true propagator (in the foreground), the ramp (on the left in the background) and the constant (on the right in the background). These scans look alike for all numbers of shot: the CLS criterion always presents a local maximum between the constant and the true propagator and is almost flat between the ramp and the constant, and the MBTT criterion always presents a nice valley going down to the true propagator. Thus, an increase of the number of shots does not change the behavior of the criterion on this particular triangle. Of course, these scans only give a very narrow idea of the full surface in V (dimension 40401) or even in V_s (dimension 169), and minimization on the triangle would not be very difficult, but this would suppose that one already knows the solution as the true propagator is a vertex of the domain.

Table 3 shows significant improvement in the quantitative results for the MBTT formulation already with the 9-shot set, and up to 96% of the data can be explained with the 41-shot set. On the other hand, the CLS formulation seems to be hurt by this increase in the number of shots.

Qualitatively, Figure 7 shows that the first three layers are now almost perfectly recovered and that a significant improvement occurs with the 41-shot set for which the fourth layer appears. On the other hand, Figure 8 confirm the quantitative results of Table 3 for the S-CLS strategy.

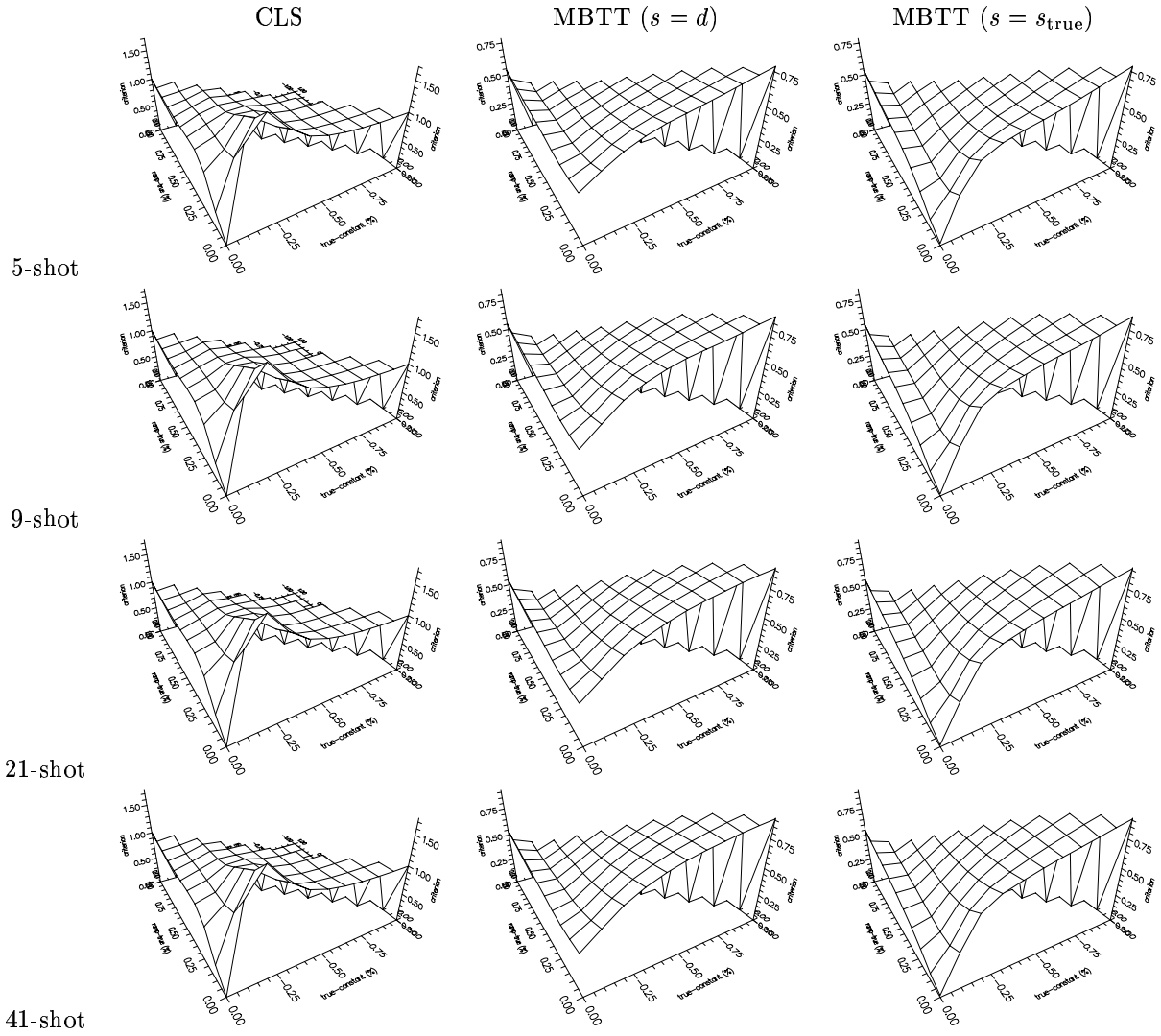

Figure 6: Scan of the CLS and MBTT criterions on the triangle joining the true propagator, the ramp propagator and the constant propagator for the 5-shot, 9-shot, 21-shot and 41-shot sets.

shots	strategy	normalized criterion	iterations	evaluations
5	S-CLS	$1 \searrow 0.152$	0+501	0+549
	MA_3-MBTT+CLS	$0.786 \searrow 0.0738 \searrow 0.0115$	90+40	108+42
9	S-CLS	$1 \searrow 0.211$	0+600	0+645
	MA_3-MBTT+CLS	$0.849 \searrow 0.0581 \searrow 0.00303$	90+40	116+42
21	S-CLS	$1 \searrow 0.257$	0+600	0+650
	MA_3-MBTT+CLS	$0.914 \searrow 0.0458 \searrow 0.00204$	90+40	116+42
41	S-CLS	$1 \searrow 0.252$	0+600	0+649
	MA_3-MBTT+CLS	$0.911 \searrow 0.0464 \searrow 0.00196$	90+40	110+44

Table 3: Optimization reports for the inversion of the Synclay data starting from the constant slowness.

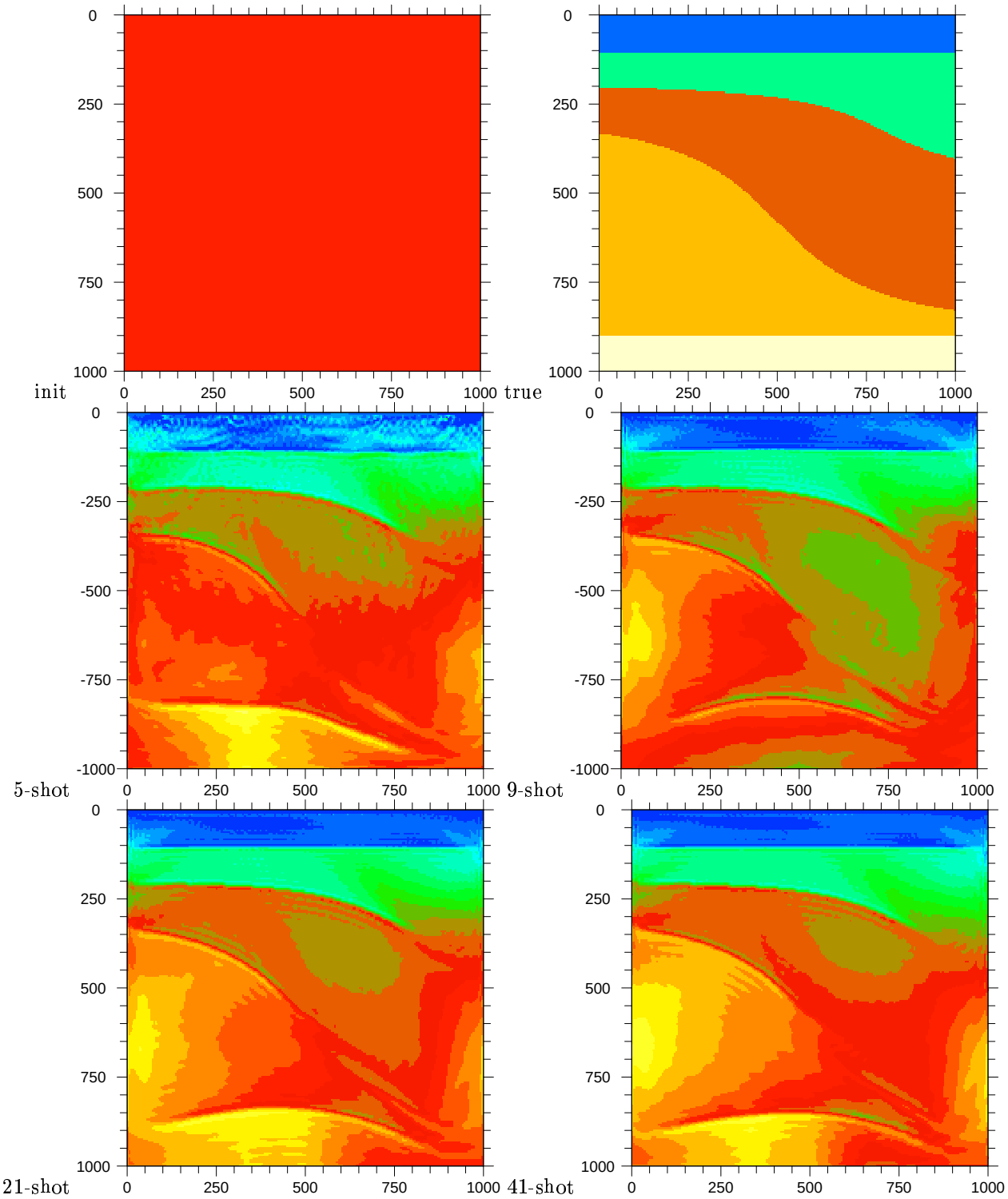

Figure 7: Full slowness after minimization from the constant for the strategy MA_3-MBTT+CLS for the 5-shot, 9-shot, 21-shot and 41-shot sets.

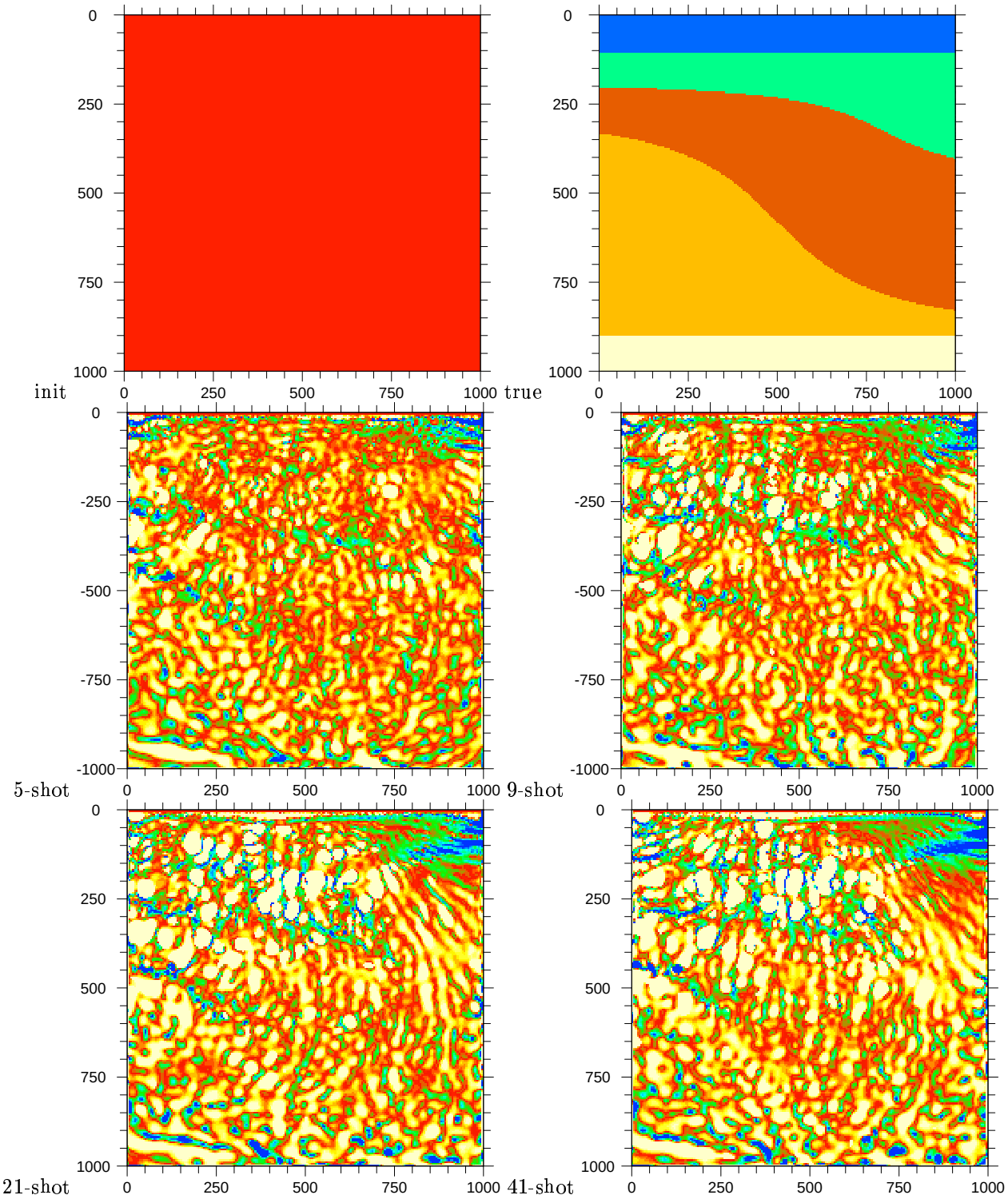

Figure 8: Full slowness after minimization from the constant for the strategy S-CLS for the 5-shot, 9-shot, 21-shot and 41-shot sets.

Conclusion

The Migration-Based TravelTime (MBTT) approach for full waveform inversion allows the minimization of the Classical Least-Squares (CLS) data misfit function by local techniques, without encountering spurious local minima, through the introduction of two new unknowns: the propagator which parameterizes the smooth background slowness and the time reflectivity which parameterizes the high-frequency components of the slowness through a migration step.

Taking advantage on a hierarchical representation of the propagator, the best optimization strategy for minimizing the least-squares criterion is to alternate minimization runs with respect to the propagator and the time reflectivity and to transfer the effort from the former to the latter as the representation of the propagator is refined.

This allows to invert a synthetic slowness model with lateral variations from a constant gradient initial guess with only 5 shot gathers, and from a constant initial guess with 41 shot gathers, while the CLS version remains trapped near the initial guess.

References

[1] G. Chavent, F. Clément, and S. Gómez. Automatic determination of velocities via migration-based traveltime waveform inversion: a synthetic data example. In *64th Annual Internat. Mtg., Soc. Expl. Geophys., Expanded Abstracts*, pages 1179–1182, 1994.

[2] G. Chavent, F. Clément, and S. Gómez. Migration-Based TravelTime waveform inversion of 2D simple structures: the Synclay model. Technical Report 3502, Inria, Rocquencourt, France, 1998.

[3] G. Chavent, F. Clément, and S. Gómez. Migration-based traveltime waveform inversion of 2D simple structures: the Synclay model. Technical report, SIGMA Consortium, Inria, Rocquencourt, France, 1998. Annual Report.

[4] Y.-H. De Roeck, G. Chavent, and R.-E. Plessix. Migration based travel time and layer stripping for inversion of VHR seismics. In *67th Annual Internat. Mtg., Soc. Expl. Geophys., Expanded Abstracts*, 1997.

[5] J.-C. Gilbert and C. Lemaréchal. Some numerical experiments with variable storage quasi-newton algorithms. *Math. Programming*, 45(3):407–435, 1989.

[6] W. W. Symes. High frequency asymptotics, differential semblance, and velocity estimation. In *68th Annual Internat. Mtg., Soc. Expl. Geophys., Expanded Abstracts*, 1998.

A The Synclay data set

The Synclay model is a synthetic 2D acoustic model. It is composed of five non horizontal layers leaning on a synclinal fold, with a shallow layer made of water, see Figure 9. The velocity and density distributions are defined on a rectangular grid of 200×200 cells with a mesh size of 5 m in both directions. The velocity successively takes the values 1500/1800/2300/3000/4000 (in m/s) and the density is constant of value 1000 kg/m^3.

The sources are located at the depth 10 m and equally distributed between the horizontal distances 100 m and 900 m, see Figure 10 and 11. The source wavelet is a Gaussian function, but, due to the free surface and to 2D propagation, the propagating signal has a peak frequency of 22 Hz and a cut frequency of 70 Hz. The 49 receivers are located at the same depth of 10 m, with a spacing of 20 m. They are fixed for all the shots. The recording time is of 1 s and is sampled at 4 ms.

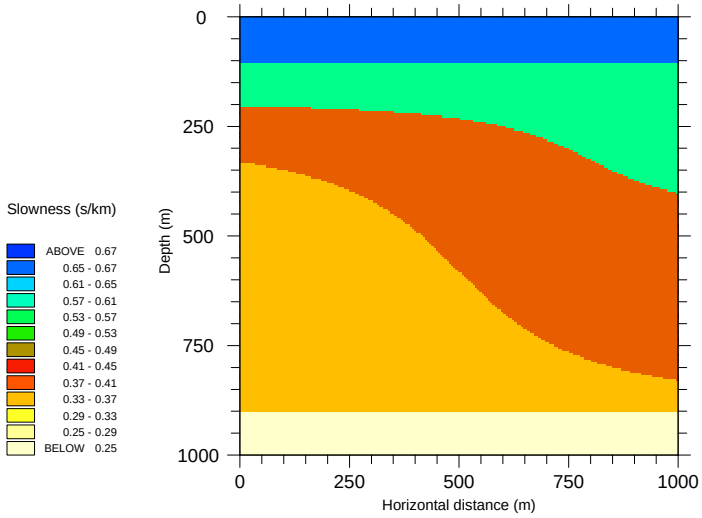

Figure 9: Synclay slowness model.

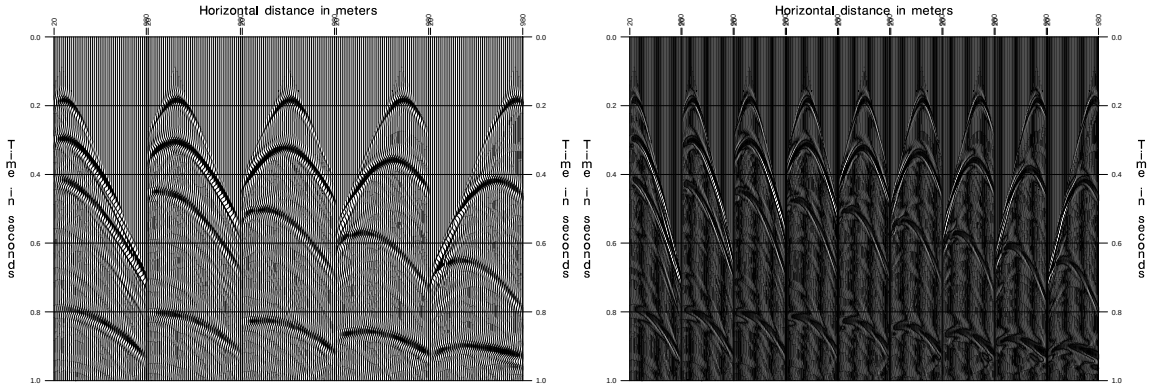

Figure 10: Synclay shot gathers. Left: 5-shot set, right: 9-shot set.

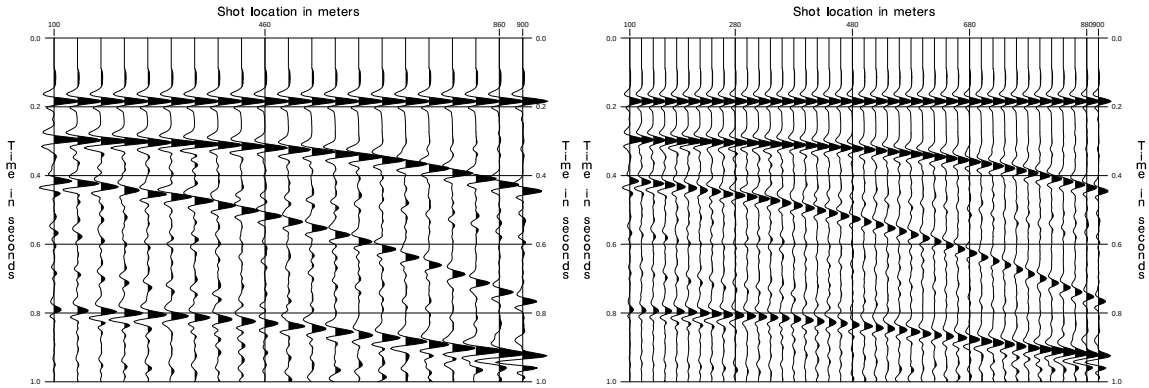

Figure 11: Synclay zero-offset gathers. Left: 21-shot set, right: 41-shot set.

Unit´e de recherche INRIA Lorraine, Technopôle de Nancy-Brabois, Campus scientifique,
615 rue du Jardin Botanique, BP 101, 54600 VILLERS LÈS NANCY
Unit´e de recherche INRIA Rennes, Irisa, Campus universitaire de Beaulieu, 35042 RENNES Cedex
Unit´e de recherche INRIA Rhône-Alpes, 655, avenue de l'Europe, 38330 MONTBONNOT ST MARTIN
Unit´e de recherche INRIA Rocquencourt, Domaine de Voluceau, Rocquencourt, BP 105, 78153 LE CHESNAY Cedex
Unit´e de recherche INRIA Sophia-Antipolis, 2004 route des Lucioles, BP 93, 06902 SOPHIA-ANTIPOLIS Cedex

Éditeur
INRIA, Domaine de Voluceau, Rocquencourt, BP 105, 78153 LE CHESNAY Cedex (France)
http://www.inria.fr
ISSN 0249-6399